

Dynamic Chiro-Optics of Bio-Inorganic Nanomaterials via Seamless Co-Assembly of Semiconducting Nanorods and Polysaccharide Nanocrystals

Saewon Kang, Gill M. Biesold, Hansol Lee, Daria Bukharina, Zhiqun Lin, and Vladimir V. Tsukruk*

This study demonstrates a novel chiral organization of multi-materials from semiconducting quantum nanorods (QNRs) co-assembled into chiral nematic polysaccharide (cellulose) nanocrystals for active manipulation of chirooptical light emission properties in elastomeric materials. Highly emissive anisotropic QNRs with dimensions and surface chemistry commensurate with those of biological nanocrystals facilitate seamless co-assembly into an integrated chiral nematic organization due to preferable enthalpic interactions and pairing processes. The resulting freestanding highly emissive bio-inorganic elastomeric materials exhibit vivid iridescence and emission with a strong optical activity that manifests itself in active and tunable chiral photoluminescence with unusually large asymmetry. Intriguingly, large-strain reversible mechanical deformation of physically crosslinked elastomers endows fully reversible alternation of helical structural configuration and corresponding linearly and circularly polarized photoluminescence. This study provides a platform to render dynamic optical functionality with reconfigurable light propagation/emission in bio-inorganic elastomers for futuristic applications in chiral lasing, biosensing, optical gauges, and holographic display.

1. Introduction

Semiconducting nanocrystals such as quantum dots (QDs), ribbons, and nanorods are intriguing candidates for efficient light emission due to their high quantum yield (QY), good thermal and chemical stability, long lifetime, narrow spectral bandwidth, and tunable emission wavelength.^[1,2] Recently, the development of chiral luminescent semiconducting nanocrystals with new optical functionalities has garnered great interest for potential applications in the fields of chiral recognition, biological sensing, 3D displays, information storage, and optical security.^[3–5] In order to utilize semiconducting

S. Kang, G. M. Biesold, H. Lee, D. Bukharina, Z. Lin, V. V. Tsukruk School of Materials Science and Engineering Georgia Institute of Technology Atlanta, GA 30332, USA E-mail: vladimir@mse.gatech.edu

6

The ORCID identification number(s) for the author(s) of this article can be found under https://doi.org/10.1002/adfm.202104596.

DOI: 10.1002/adfm.202104596

nanocrystals with optical activity, several approaches have been implemented to date, such as supramolecular assemblies,^[6] enantioselective synthesis,^[3,7,8] and chiral ligand exchange. [9-12] For example, doping achiral quantum nanocrystals into a chiral supramolecular system has opened up possibilities for the design of functional photoluminescent materials with induced chiro-optical behavior. [9,13] However, such assembly approaches require sophisticated multi-stage fabrication and render relatively weak optical activity (with an asymmetry factor of left/ right circular polarization intensity within $10^{-2} - 10^{-4}$). [11,12,14,15]

Coupling the optoelectronic properties of individual semiconducting nanocrystals with photonic structures could enable the development of novel optically functional materials with circularly polarized light (CPL) emission with large asymmetry of circular polarization. Chiral biopolymers, such as polysaccharides, DNA, and

proteins, can be attractive bio-templates that provide optical elements with built-in solid-state chiral organization. Among polysaccharide nanocrystals, cellulose nanocrystals (CNCs) with high aspect ratio and spindle-shape are most widely explored for chiral bio-templates.[16,17] Aqueous CNC dispersions can form a chiral nematic liquid crystal (LC) phase with a lefthanded helical structure.[18] Integrating optically active synthetic components into a helical structure can create nanostructures with intriguing optical functionalities via a host-guest coassembly process. [19-21] Among these appealing nanostructures, QDs, metal nanoparticles, and organic dyes have been employed to control the light polarization of chiral photonic structures, resulting in chiral photoluminescence. [22-26] For instance, chiral emissive CNC composites incorporating semiconducting QDs (i.e., carbon dots, CdSe QDs) have been fabricated, and the resulting chiral photonic composites exhibited selectively reflected left-handed CPL, leading to strong righthanded emission.^[21,27] Although this synergistic integration endows the composites with the unique optical functionality of emissive QDs, the composites exhibit weak emission with static optical activity and thus a limited ability to adapt quickly to a changing environment.





www.afm-iournal.de

As known, without tailoring complementary QD-CNC surface chemistries, doped QDs are usually excluded from LC phases of CNCs due to thermodynamic incompatibility. [28] For example, MacLachlan et al. demonstrated the selfassembly of CdS QDs into chiral nematic CNC-template silica, that demonstrated the maximum doping concentration of QDs without a passivation of polyvinyl alcohol (PVA) about 1.4% with substantial aggregation observed at higher concentration.^[29] Passivating emissive QDs with polyethylene glycol (PEG) has been shown to effectively enhance interactions with CNCs, enabling to avoid aggregations, and render uniform intercalation. [21,27] However, higher concentrations of emissive QDs has been shown to disrupt chiral organization, leading to optical loss and destruction of photonic organization. [30,31] In particular, increasing the volume fraction of QDs in cholesteric CNC composites leads to phase separation due to thermodynamic instability in the composite system. [28,32,33] Moreover, owing to disparities in shapes, symmetries, and surface chemistries, nanocrystals incorporated in LC systems tend to be concentrated at boundary regions, which decreases the stability of LC phases. To mediate this issue, active dopants need to be sufficiently small enough to be intercalated into limited interstitial free volumes between densely packed nanocrystals.^[34] Shape complementarity can determine the self-organization based on complex collective colloidal interactions, such as Coulombic, van der Waals, hydrophobic, and hydrogen bonding and thermodynamicallydriven forces to tailor structural complexity in nanoparticulated composite systems, enabling unusual shape-dependent optical phenomena.[35-38]

Therefore, careful consideration of QD size and dimensions in relation to the interstitial free volume is required for stable co-assembly of QDs with the LC phases.

Here, we demonstrate chiral and emissive bio-inorganic composites, comprised of semiconducting core-shell CdSe/ CdS quantum nanorods (QNRs) integrated into a chiral nematic organization of CNCs via seamless co-assembly and additionally crosslinked into elastomeric matrices. The interfacial interactions between water-soluble ONRs and CNCs with identical geometrical dimensions enable spontaneous intercalation of the optically active inorganic components into the chiral nematic biological organization for minimization of excluded volume without phase separation even at high QNR concentrations of 3.75 wt%. The resulting bioinorganic structures (CNC-QNR) embedded in an elastomer matrix possess an intense photonic appearance and bright CPL emission with large asymmetry due to the CNC-induced helical arrangement of QNRs. In addition, this unique chiral organization enables the generation of a mechanically stable elastomeric LC polydomain texture, leading to the formation of the elastomeric bio-inorganic composites with robust structural reconfigurability and an anisotropic Poisson's value under uniaxial mechanical extension up to 70%. Mechanically-induced twisting of these bio-inorganic materials results in a reversible structural reconfiguration from chiral nematic to nematic phase, allowing the elastomeric composites to possess tunable optical activity with fast reversible switching from circularly to linearly polarized photoluminescence under strains.

2. Results and Discussion

2.1. Co-Assembly of ONRs and CNCs

CNC dispersions were synthesized from soft-wood pulp via a well-established hydrolysis method (Figure S1, Supporting Information). [39,40] Emissive CdSe/CdS core-shell QNRs were synthesized via a seeded hot injection route.[41] Subsequently, ligand-exchange of as-synthesized QNRs was conducted to replace original hydrophobic surface ligands (a combination of octadecylphosphonic acid and hexylphosphonic acid) with hydrophilic ligands (diaminopropane), yielding water-soluble core-shell QNRs (see Experimental Section). The short molecule 1,3 diaminopropane was chosen as a ligand to render superior water solubility as well as to facilitate intercalation of the ONRs into the CNCs (Figure S2, Supporting Information). The outer positively charged amine groups provided by the ligands impart face-to-face contact between the anisotropic QNRs and individual CNCs with negatively charged sulfate groups via attractive Coulombic interactions.[42] The decrease in zeta-potential from -47.2 ± 1.4 mV for bare CNC dispersion to -29.7 ± 1.1 mV for bio-inorganic CNC-QNR suspension confirms stable colloidal suspensions and spontaneous co-assembly (Figure S3, Supporting Information).

The well-defined high aspect ratio and compatible surface chemistry of QNRs allow them to orient along a helical axis of CNCs and to form a chiral nematic structure due to entropic force-induced seamless intercalation (**Figure 1**a). ^[42] A transmission electron microscopy (TEM) image shows as-synthesized QNRs with high aspect ratio and uniform size very similar to those for pristine CNCs (Figure 1b). Indeed, high-resolution atomic force microcopy (AFM) images demonstrate uniform individual inorganic nanorods and biological nanocrystals, showing identical needle-like shapes with a similar diameter of ≈5.5 nm and an aspect ratio of ≈18 (Figure 1c,d; Figure S4, Supporting Information).

Next, we measured the absorption and photoluminescence spectra of the QNRs dispersed in hexane and water (Figure 1e; Figure S5, Supporting Information). Both samples showed strong absorption in UV region (Figure S5, Supporting Information). We did not observe any defect emission with same intensity in photoluminescence spectra, indicating defect-free surface of the QNRs (Figure 1e). The absolute photoluminescence quantum yield (PLQY) of CdSe/CdS core-shell QNRs dispersed in water was found to be 5.5% (see Experimental Section). This value is somewhat lower than that reported for core-shell dots due to increasing numbers of trap states on the CdS region of high aspect ratio of nanorods.^[41] Moreover, the water-soluble QNRs showed excellent photostability in water (Figure 1f). Furthermore, as-mixed CNC-QNR suspension showed bright photoluminescence under 365 nm light irradiation (Figure 1g).

2.2. Bio-Inorganic CNC-QNR Composite Elastomeric Films

Free-standing CNC-QNR composite films were fabricated via evaporation-induced self-assembly process (Figure 2a). [21,39] The resulting films showed a dominant yellow color and excellent mechanical flexibility. A polarized optical microscopy of these

www.advancedsciencenews.com www.afm-journal.de

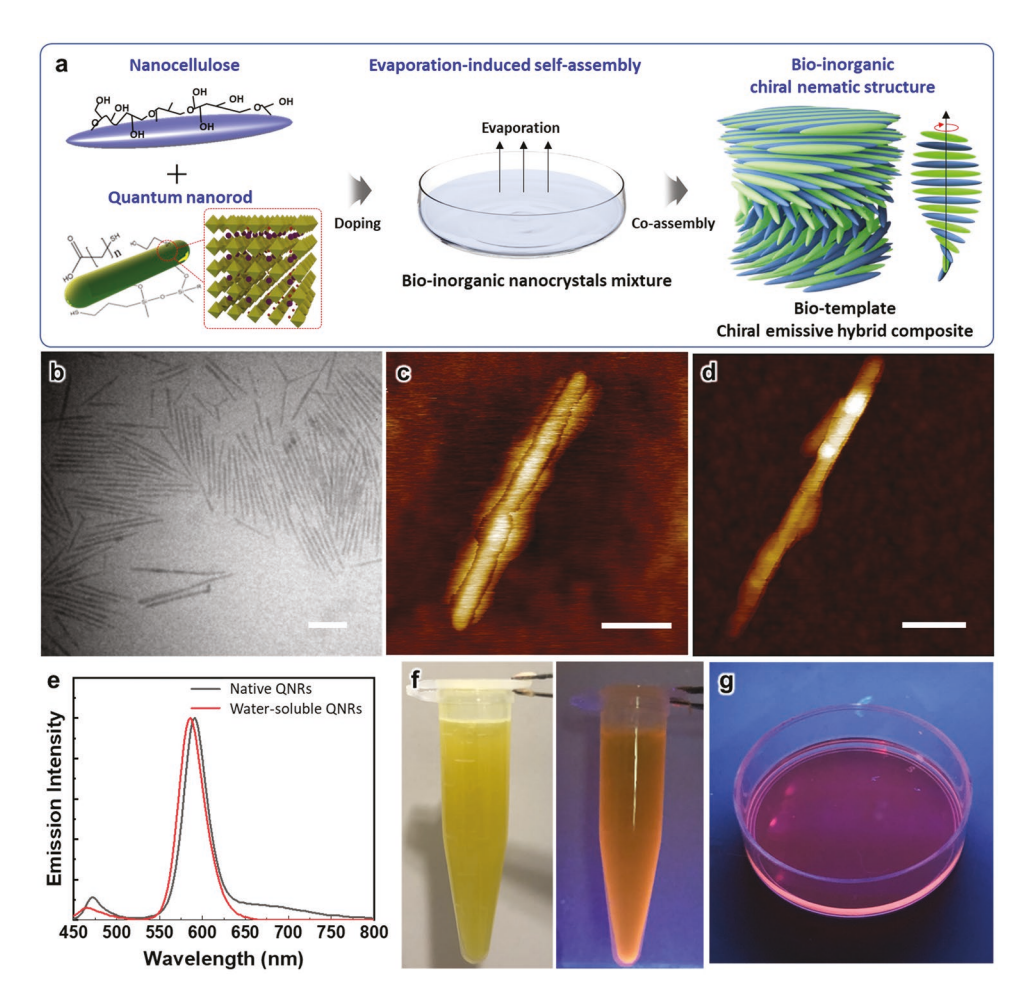


Figure 1. Co-assembly of QNRs and CNCs. a) Schematic of synthesis for highly emissive bio-inorganic chiral nematic organization, consisting of CNC and water-soluble CdSe/CdS QNRs via evaporation-induced self-assembly process. Chiral nematic CNC structure as bio-templates enabled QNRs to be arranged with helical ordering caused by seamless co-assembly, generating strong active circularly polarized light emission with strong optical activity. b) TEM image of individual CdSe/CdS QNRs with needle-like shape morphology. Scale bar is 50 nm. AFM images of c) single CdSe/CdS QNR and d) individual CNC, coated on silicon substrates, respectively. Both scale bars indicate 50 nm. e) Comparison of photoluminescence spectra for CdSe/CdS core-shell QNRs dispersed in organic solvent and ligand-exchanged QNRs dispersed in water. f) Photographs of QNRs dispersed in water under natural light (left) and under 365 nm light (right). g) Photographs of as-mixed CNC-QNR suspension on Petri dish (30 mm × 15 mm) under 365 nm UV light.

films displays birefringence with multiple microscopic LC tactoids (Figure 2b).^[43] A scanning electron microscopy (SEM) image of cross-sections of the films shows traditional Bouligand morphology with sub-micron layered organization without signs of microscopic phase separation, facilitating uniform bioinorganic morphology (Figure 2c,d).^[44]

As a control experiment, chiral CNC composite films combined with conventional, spherical core-shell CdSe/ZnS QDs were fabricated by mixing CNC suspension with QD at a concentration of 3.75 wt%, followed by the self-assembly (Figures S6 and S7, Supporting Information). The resulting CNC-QD films with photonic appearance exhibited negligible fluorescence, which can be attributed to QD aggregation that leads to fluorescence quenching and high optical loss (Figure S8 and S9, Supporting Information). In stark contrast, the CNC-QNR films displayed bright fluorescence (Figure S8, Supporting Information).

In addition, high-resolution AFM images confirm the existence of multiple LC tactoids with highly aligned CNC-QNR nanostructures (Figure 2e,f; Figure S9, Supporting Information). Generally, during the film formation, negatively charged CNCs are stacked with a small twisting angle (1–5°) to construct chiral nematic organization from stacked monolayers due to repulsive forces between neighboring nanocrystals. [18] We suggest that the co-assembly of the positively charged nanorods into the helicoidal CNC organization is dominated by shapedriven directional entropic interactions and Coulombically-driven enthalpic contribution which enable preferential alignment of neighboring biological and inorganic nanocrystals, leading to seamless co-assembly of nanorods and nanocrystals into stacked organization (Figure 2d). High-resolution SEM images show uniform long bundles and modest contrast in backscattered images caused by incorporated inorganic nanorods (Figure S10, Supporting Information). [45–49]

To further verify nanorod-nanocrystal distribution, quantitative nanomechanical mapping (QNM) was conducted to investigate surface morphologies and to map the nanomechanical properties (Figure S11, Supporting Information). In a QNM

www.advancedsciencenews.com www.afm-journal.de

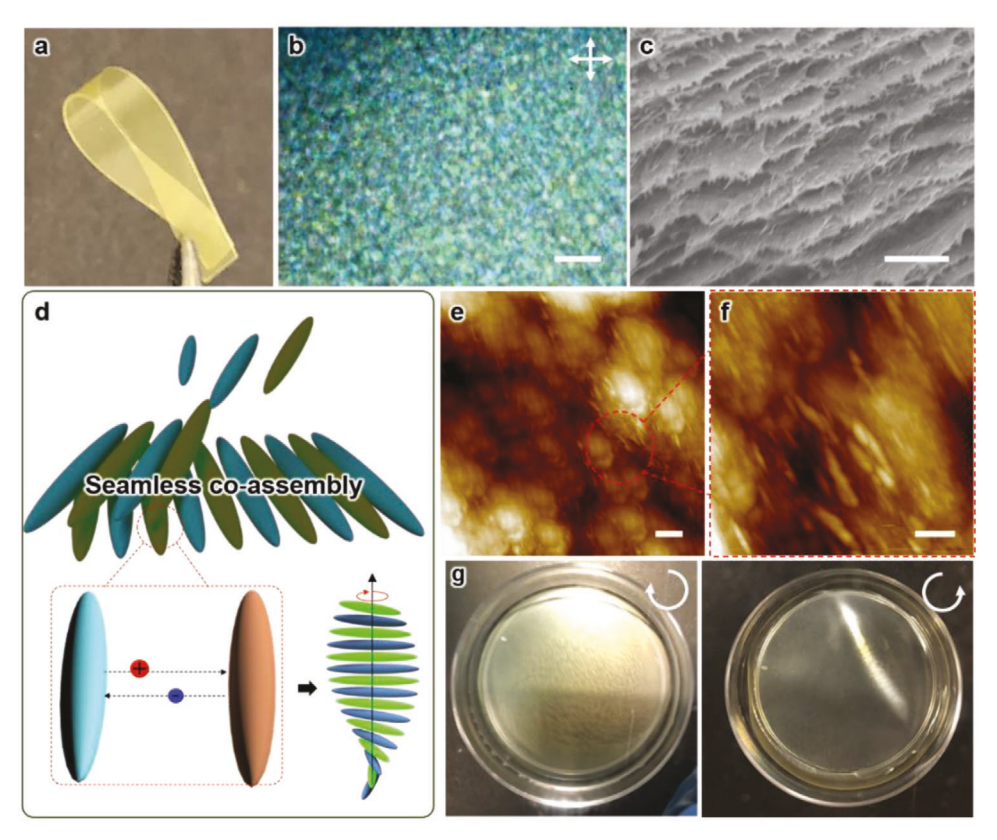


Figure 2. Bio-inorganic CNC-QNR composite films: a) Free-standing bendable chiral nematic CNC-QNR film. b) Polarized optical microscope image of assembled hybrid chiral CNC-QNR composite film under bright-field mode using cross-polarizer. The scale bar is $10 \mu m$. c) SEM image of a cross-section of the interior layer of the CNC-QNR composite films with periodic chiral organization. The scale bar is $1 \mu m$. d) Intercalation behavior of core-shell QNRs into chiral nematic organization of CNC due to electrostatic interactions. e,f) AFM images of as-fabricated CNC-QNR films with microscopic polydomains. Scale bars are e) 200 and f) 100 nm. g) As-fabricated CNC-QNR films viewed with left-handed and right-handed circular polarizers.

mode, we observe that some nanocrystals that are aligned face-to-face in a well-ordered phase showed a slightly lower elastic modulus compared with that of neighboring nanocrystals.^[50,51] These results indirectly support that QNRs are arranged in face-to-face with neighboring CNCs.

Notably, excessive concentration of positively charged QNRs above 7 wt% affects ionic strength in CNC dispersion, leading to an interruption in the local twisting power of CNCs with substantial particle aggregations and phase separation, causing the interference in the formation of chiral nematic LC phase with diminishing structural photonic appearance and non-uniform organization (Figures S12 and S13, Supporting Information).^[34]

2.3. Dynamic Structural Reconfiguration of Bio-Inorganic Chiral Elastomers

As known, the unique macroscopic helical organization of CNCs provides an efficient way to control the polarization of active light emission generated by dynamic reconfiguration of QNRs driven by change in chiral templates. In fact, uniaxial deformation of chiral nematic phase in an elastomeric matrix can lead to a transition from chiral nematic structure to an unidirectional nematic structure, resulting in dramatic structural color change under a cross-polarizer due to reversible birefringence changes. [52]

To study the mechano-optical behavior, water-soluble QNR solution (1.5 mg) was mixed with polyurethane (PU, 320 mg) dispersed in water, followed by further mixing with CNC suspension (40 mg) before film formation induced by evaporationinduced self-assembly (see Experimental Section). As-fabricated free-standing film including CNC-QNR embedded into an elastomeric matrix was further cross-linked by annealing at 70 °C for 2 h. The resulting CNC-QNR-PU elastomeric films retain vivid structural color under natural light and bright light emission under 365 nm UV light (Figure 3a). A polarized optical microscopy image shows conventional texture of random LC tactoids (Figure 3b). Strong positive circular dichroism (CD) signals confirm the presence of a left-handed chiral nematic organization and different optical density under left- and right-handed circular polarizers in the CNC-QNR-PU films (Figure 3c; Figure S14, Supporting Information).

The resulting chiral elastomeric films can be reversibly stretched up to 120% (Figure S15, Supporting Information). The films show excellent mechanical performance with an ultimate strain of 119 \pm 12% and a strength of 9.9 \pm 1.1 MPa, compared to that of PU elastomer containing pure QNRs with an ultimate strain of 441 \pm 130% and a strength of 3.5 \pm 0.7 MPa. The CNC-QNR-PU films possess an elastic modulus of 863 \pm 84 MPa, which is significantly greater than that of QNR-PU elastomeric films (49.1 \pm 8.1 MPa) (Figure S15, Supporting Information).

www.afm-journal.de

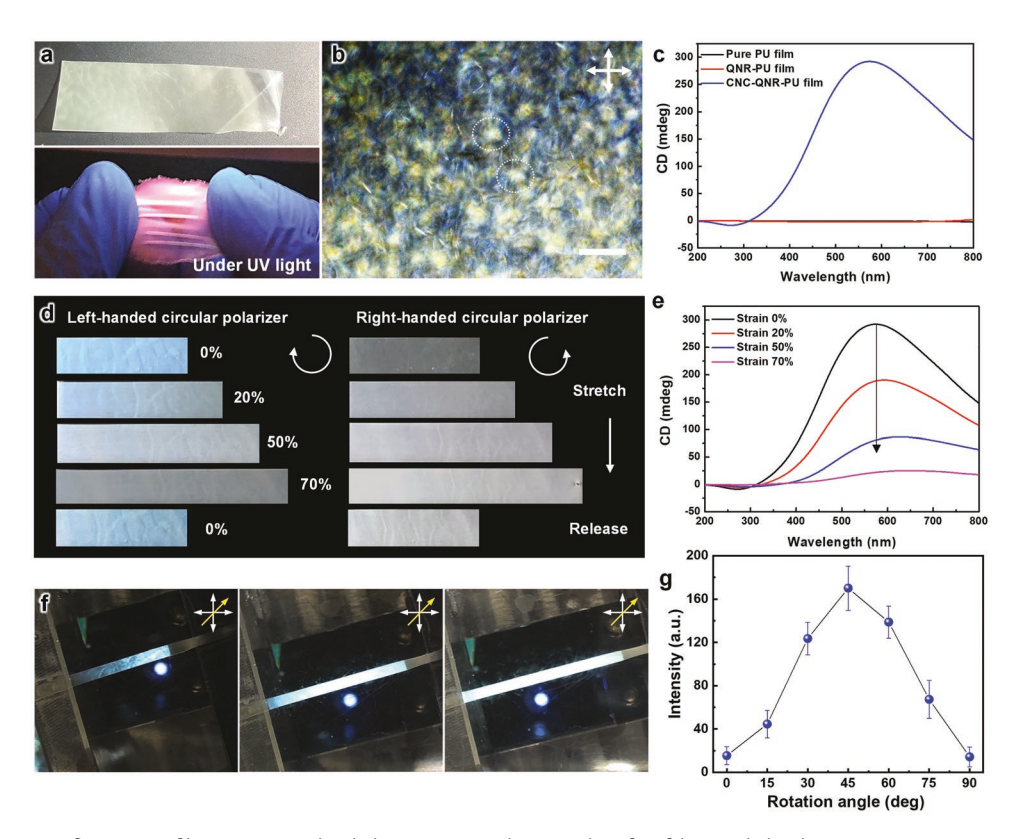


Figure 3. Dynamic reconfiguration of bio-inorganic chiral elastomers. a) Photographs of as-fabricated chiral CNC-QNR composite embedded in elastomeric matrix under visible light (top) and 365 nm UV light (bottom). b) Polarized optical micrograph of chiral CNC-QNR-PU films, showing multiple small photonic domains. The scale bar is 10 μm. c) CD spectra of as-fabricated PU, QNR-PU, and CNC-QNR-PU elastomeric films. d) The change in photonic appearance of chiral elastomeric composite films viewed by left- and right-handed polarizers. Structural re-arrangement of CNC-QNRs in chiral organization in response to an increase of mechanical strain caused dynamic chiroptical properties. e) CD spectra of chiral elastomeric films stretched in varying mechanical strain. The films were kept stretched during the measurement. f) Photographs of chiral CNC-QNR-PU films placed between crossed polarizers with an increase of mechanical strain, rotated to 45° against the direction of crossed polarizers. g) Angle-dependent-polarized light transmission of stretched CNC-QNR films measured by hyperspectral imaging. The data were collected from three different samples using hyperspectral optical imaging under crossed polarizers.

The enhanced strength of CNC-QNR-PU composites can be related to filler-reinforcement effect with increasing total concentration of stiff additives (around ≈10 wt%) with the formation of densely physically cross-linked PU matrix.

Interestingly, the chiral organization of the CNC-QNR-PU elastomers leads to anomalous volume change with directiondependent Poisson's ratio when stretched up to 70% (Figure S16, Supporting Information). The Poisson's ratio (v), defined by the ratio of the lateral/longitudinal strain, is close to zero (v = 0.1) in the in-plane (width) direction whereas a regular value of 0.44 is obtained in the out-plane (thickness) direction. This is divergent from the deformational properties of pure PU elastomer which maintains isotropic deformation with v = 0.36 in out-plane and v = 0.42 in-plane directions (Figure S16, Supporting Information).[53] We suggest that this unusual anisotropic mechanical contraction can be attributed to the chiral nematic geometry that "built-in" to the elastomeric matrix, promoting anisotropic stress distribution as those observed in anisotropic foam-like morphologies.^[54-57] The anisotropic organization leads to significant enhancement of mechanical properties (modulus and stiffness) along the orientation direction of nanocrystals.^[58] Chiral bio-inorganic CNC-QNR nanostructures composed of anisotropic layers stacked along the helical axis that include

orthogonal structures enable to anisotropic mechanical contraction such as those observed for cork-type materials.^[52,54] For these anisotropic materials, the Poisson's ratio is close to zero due to high stiffness in the deformed direction while shrinkage occurs in the softer orthogonal direction.^[59,60]

To observe structural changes of the CNC-QNR-PU elastomer under mechanical deformation, the photonic appearance with birefringence was monitored under increasing mechanical strain (Figure 3d). The pristine film exhibited vivid structural color with the anisotropy in optical density viewed by leftand right-handed circular polarizers, which can be attributed to the left-handed helical nature of chiral CNC organization (Figure 3d; Figure S14, Supporting Information). As mechanical strain increased, the difference in optical density gradually decreased and eventually disappeared at 70% strain (Figure 3d). After releasing stress, the color of the films rapidly returned to their original appearance. Correspondingly, a positive CD peak near 570 nm observed in the un-stretched films gradually decreased with increasing mechanical strain and the CD peak recovered after stress was removed (Figure 3e; Figure S17, Supporting Information).

To investigate the reconfiguration of the elastomeric films induced by mechanical deformation, the stretched film was



www.afm-iournal.de



placed at 45° angle to crossed polarizers (Figure 3f). Under this orientation conditions, the intensity of transmitted light gradually increased with increasing mechanical strain. This result suggests that the films in a stretched state possess anisotropic LC ordering, induced by the transition from chiral nematic to unidirectional nematic organization. [50] For further verification of this transition, polarized light transmission of the films was collected using hyperspectral microscopy under crossed polarizers (Figure S18, Supporting Information). When the stretched film was rotated between the crossed polarizers, the maximum transmitted light intensity was recorded at a 45° angle to crossed polarizers, indicating anisotropic birefringence with an optical axis aligned along the stretching direction (Figure 3g; Figure S18, Supporting Information).

2.4. Mechanically-Triggered Dynamic Light Polarization

It is notable that this structural reconfiguration triggered by mechanical deformation can lead to fast and reversible circular-to-linear photoluminescence transition due to alternation of nanorod orientation in the chiral nematic matrix (Figure 4a). For pure QNRs coated on a quartz, unpolarized photoluminescence emission was observed at 600 nm, and there is no difference in the photoluminescence intensity measured using left- and right-handed circular polarizers (Figure S19, Supporting Information). In contrast, the CNC-QNR-PU films generated strong CPL emission with optical rotation. The intensity of the left-handed CPL is higher than that of the right-handed CPL, revealing that the co-assembly within chiral CNC structures facilitates CPL emission (Figure 4b).

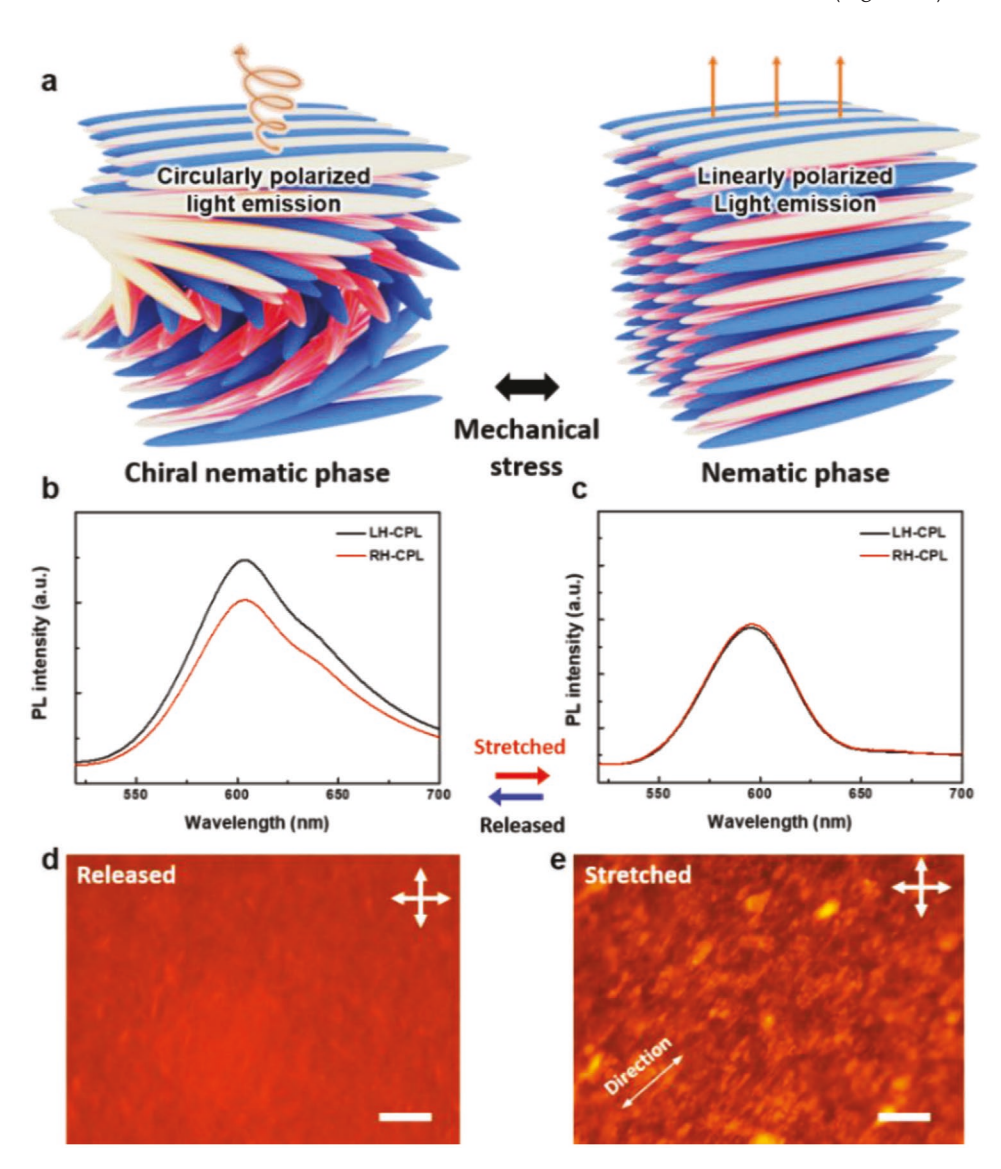


Figure 4. Mechanically-triggered polarization changes of emitted light. a) Structural reconfiguration of chiral bio-inorganic CNC-QNR elastomeric films in response to mechanical stimuli, leading to reorientation of CNC-QNR from chiral nematic to nematic structure when the film is stretched. Photoluminescence spectra of b) unstretched and c) stretched CNC-QNR elastomeric composite film measured using left- and right-handed circular polarizer. Fluorescent optical images of d) unstretched and e) stretched CNC-QNR-PU films at 70% strain. The arrow indicates stretching direction. The scale bar is 10μm.





www.afm-journal.de

Furthermore, based on the difference in the left-handed and right-handed CPL spectra, the asymmetry factor was calculated as $|g_{\text{lum}}| = 2 \times (I_{\text{L}} \cdot I_{\text{R}})/(I_{\text{L}} + I_{\text{R}}),^{[26,61]}$ where I_{L} and I_{R} are the emission intensities collected through the left- and right-handed CPL, respectively. The asymmetry factor reached 0.2 in non-stretched films, orders of magnitude higher than common values for chiral-induced QDs produced by various methods. [11,12,15] Notably, the absolute PLQY of CNC-QNR-PU films was observed to be 6.5%, which is an order of magnitude higher than that of other polymer-based emissive chiro-optical films. [62–64] Remarkably, when the films were stretched, they showed no asymmetric CPL emission, yet linearly polarized light emission parallel to the stretching direction was observed (Figure 4c; Figure S20, Supporting Information).

The fluorescent microscopy of the stretched films viewed under the crossed polarizers demonstrates unidirectional alignment of CNC-QNRs along the direction of mechanical strain, resulting in linearly polarized light emission (Figure 4d,e). For further verification of linearly polarized photoluminescence, the photoluminescence of the stretched films was analyzed by a hyperspectral microscopy equipped with a linear polarizer (Figure S20, Supporting Information).

Photoluminescence intensities of the stretched films were collected with varying polarization angles from 0° to 180° (Figure S20, Supporting Information). The stretched films exhibited minimum photoluminescence intensity when the stretched direction of the films was perpendicular to the direction of the linear polarizer. This result supports that the chiral phase of CNC-QNR nanostructure changes to unidirectional nematic organization along the direction of mechanical strain, leading to linearly polarized light emission (Figure S20, Supporting Information).^[65]

3. Conclusion

In conclusion, chiral emissive bio-inorganic elastomeric materials were crafted via a host-guest co-assembly of inorganic nanorods and biological nanocrystals with nearly identical aspect ratios and complementary surface chemistries. Specifically, the commensurate dimensions and surface chemistry of CdSe/CdS QNRs enabled superior intercalation into the chiral nematic CNC phase. This rendered them to orient along the left-handed helical axis in the chiral CNC media without phase separations due to favorable electrostatic attraction and entropic force-driven self-assembly.

Chiral CNC-QNR-PU elastomers undergo mechanically-triggered transition from chiral helical organization to unidirectional nematic morphology and possess anisotropic elastic properties with a near-zero Poisson's ratio in the in-plane direction due to the helicoidal geometry of the built-in elastomeric matrix. Reversible mechanical deformation induced a reversible switch from circularly polarized to linearly polarized light emission due to stress-induced twisting of CNC-QNR embedded in the elastomeric matrix, leading to a mechanically-controlled transition from chiral nematic to unidirectional nematic organization. We suggest that a reversible stress-triggered reconfiguration of chiral emissive Bouligand structure found

in the CNC-QNR-PU elastomers can be further extended for designing functional dynamic photonic elastomeric materials for CPL-based holography, mechanosensing, optical coding, and chiral sensing.

4. Experimental Section

Chemicals: Trioctylphosphine oxide (TOPO, 99%, Sigma Aldrich), trioctylphosphine (TOP, 97%, Sigma Aldrich), selenium (Se, 99.999%, Alfa Aesar), octadecylphosphonic acid (ODPA, 97%, Beantown Chemical), hexylphosphonic acid (HPA, 99%, Beantown Chemical), 1-octadecene (ODE, 90%, Acros Organic), zinc acetate dihydrate (Zn(acetate), ACS, Alfa Aesar), oleic acid (90%, Alfa Aesar), sulfur (99.5%, Alfa Aesar), hexane (ACS), dodecanethiol (98%, Alfa Aesar), diaminopropane (99%, Acros Organic), CdO (98.9% Alfa Aesar), and 1-dodecanthiol (98% Sigma Aldrich). All chemicals were used as received.

Synthesis of CdSe Seeds: 3.0 g TOPO, 0.280 g ODPA, and 0.060 g CdO were added into a 25 mL three neck flask and heated to 150 °C under vacuum for 1 h. The flask was then purged with nitrogen, and the temperature was increased to 300 C. Once the CdO was fully dissolved, 1.50 g TOP was injected into the flask. The temperature was then increased to 380 °C, at which point a solution of 0.058 g Se and 0.360 g TOP was injected. Immediately following injection, the heating mantle was removed. Once cooled, the nanocrystals were precipitated with methanol and were washed by repeatedly dispersing in toluene and precipitating in methanol. Once fully washed, the CdSe seeds were dispersed in TOP.

Synthesis of CdSe/ZnS QDs: The gradient composition CdSe/ $Cd_{1-x}Zn_xSe_{1-y}S_y/ZnS$ core/shell QDs were synthesized in a method similar to that previously reported. [66] 5 mmol CdO, 10 mmol zinc acetate, 25 mL oleic acid, and 75 mL ODE were placed in a three neck flask and nitrogen was passed through for 5 min. The solution was then degassed at 150 °C for 3.5 h. While degassing, 1 mL of 1 M Se/TOP solution and 5 mL of 2 m S/TOP solution were made. After degassing, the reactor was purged with nitrogen gas and the temperature was raised to 300 °C for 30 min. After 30 min, 1 mL of 1 M Se/TOP solution was injected. The reaction was allowed to continue at 300 °C for 5 min. After 5 min, 1.5 mL dodecanthiol was injected drop by drop. Twenty minutes after the addition of dodecanethiol, 5 mL of the 2 $\,\mathrm{M}$ S/TOP solution was injected and the heating mantle was removed. 50 mL of hexane were added once the temperature reached 70 °C. The nanocrystals were purified by precipitating with acetone and were redispersed in toluene three times.

Synthesis of CdSe/CdS Nanorods: To synthesize CdSe/CdS nanorods, 3 g TOPO, 0.290 g ODPA, 0.080 g HPA, and 0.091 g CdO were placed in a three neck flask and heated to 150 °C under vacuum for 1 h. After 1 h, the flask was purged with nitrogen, and the temperature was raised to 350 °C. Once the temperature reached 350 °C, 1.5 g TOP was injected into the flask. The temperature was allowed to return to 350 °C, at which point a mixture of 0.120 g S, 1.5 g TOP, and 200 μL of the seed CdSe QDs in TOP was injected. The solution was then held at 350 °C for 8 min, after which time the heating mantle was removed. Once the sample cooled to $\approx\!70$ °C, hexane was added to the solution to ensure it stayed at liquid phase at room temperature. Once fully cooled, the nanorods were precipitated with methanol and redispersed in toluene.

Ligand Exchange: The same procedure was used on both the nanorods and QDs. 2 mL of nanocrystals in hexane were precipitated with 13 mL acetone in a 15 mL centrifuge tube, and centrifugated for 5 min at 6500 RPM. The precipitate was then collected and the supernatant was discarded. 2 mL of diamino propane was then added to the precipitate in the centrifuge tube and vigorously shaken until redispersed. The solution was then centrifuged again and the precipitated nanocrystals were dispersed in water.

Preparation of CNC Suspension: All CNCs used in this study were obtained from the soft wood pulp. The dried soft wood pulp $(17.00~{\rm g})$



www.afm-journal.de

ADVANCED FUNCTIONAL MATERIALS

was hydrolyzed in sulfuric acid (16 mL of a sulfuric acid per gram pulp) with a concentration of 64 wt% at 45 °C with constant stirring for 60 min. The resulting as-synthesized yellow suspension was diluted to ten times volume with DI water to quench the hydrolysis. The solution was left untouched for 12 h, during which the hydrolyzed wood pulp separated from the DI water. The upper solution was discarded and the remained suspension was purified twice by centrifuging at 6000 rpm for 5 min to remove extra sulfuric acid. Afterward, the dialysis process was conducted on the re-dispersed suspension with dialysis membrane tubes with molecular weight cutoffs of 14 kDa for 1 week (the water was changed every 6 h) until the pH value of the water was constant. After dialysis, the cellulose dispersion was centrifuged at 11 000 rpm for 20 min, and the aqueous suspension was kept, while the remaining semisolid aggregate at the bottom was discarded. Ultrasonication was carried out on the obtained CNC dispersion with a tip sonicator for 20 min (Qsonica Q125, 700 W) at 50% amplitude. Then the CNC dispersion was concentrated by controlled water solution evaporation.

Self-Assembly of Bio-Inorganic CNC-QNR Composite Films: 1.5 mg of QNRs was added in 2 mL of concentrated CNC dispersion (2 wt%). Subsequently, bio-inorganic CNC-QNR solution was mixed with stirring for 1 h and sonicated for 30 min in the bath for uniform distribution of QNRs. The mixture was then drop-cast into polystyrene Petri dishes (35 mm in diameter) to allow for evaporation-induced self-assembly in ambient condition. The chiral bio-inorganic composite solid film was then self-assembled after 2 days.

Preparation of Bio-Inorganic CNC-QNR-PU Elastomeric Film: 300 μL of water-soluble QNRs (0.5 wt%) was added into 4 mL of polyurethane (8 wt%) dispersed in water and mixed with stirring for 2 h. Then, 2 mL of concentrated CNC dispersion (2 wt%) was added into the mixture, followed by stirring for 2 h. The weight ratio of CNC:QNR was fixed to 96.25:3.75%. The mixed solution was drop-cast into polystyrene Petri dishes (35 mm in diameter) and dried for 3 days. Homogeneous and iridescent chiral bio-inorganic CNC-QNR-PU elastomeric films were obtained via evaporation-induced self-assembly under ambient condition. As-prepared CNC-QNR-PU films were further cross-linked by annealing at 70 °C for 2 h in the oven.

Characterization: Optical images were collected using an Olympus BX51 microscope in the reflection mode and under bright field with crossed polarizers to observe the surface morphologies of bio-inorganic CNC-QNR films. The morphologies of the as-prepared QNRs were investigated with a IEOL CX-II electron microscope operated at 100 keV.

AFM was conducted to investigate individual CNCs and QNRs on silicon substrates using Bruker Dimension Icon in tapping mode at scanning rate of 0.7 Hz. [67] The AFM images were acquired using AFM probes (MikroMasch, HQ:XSC11/ALBS) with a spring constant of 2.7 n m $^{-1}$ and a tip radius of $\approx\!8$ nm in air. Zeta-potential of CNC-QNR solution was measured as a function of QNR concentrations with a Malvern Zetasizer Nano ZS.

To measure mechanical properties of CNC-QNR-PU elastomeric films, all films were cut into 5 mm x 30 mm samples. A tensile tester (Shimadzu EZ-SX 500 N) was utilized to obtain the tensile stress–strain curves of the films with a speed of 0.1 mm s⁻¹ under ambient condition. To calculate Poisson's ratio of the films, the film width and thickness for four samples were measured using digital caliper.

The CD spectra were collected using an Applied Photophysics Chirascan plus. Optical properties of pure QNRs and QDs were analyzed using UV-vis-NIR (a Shimadzu UV-2600). The photoluminescence spectra of pure core-shell QNRs and QD solutions were obtained with a PerkinElmer LS 55 fluorescence spectrometer under 365 nm excitation. The absolute PLQY of QNR and QDs was measured with a Hamamatsu Quantaurus QY Plus with an excitation wavelength of 365 nm according to the usual procedure. [68] Circularly polarized photoluminescence was characterized using a Shimadzu UV 2450 under a broadband left- and right-handed circular polarizers, respectively. Hyperspectral optical intensity detection system was utilized to measure angle-dependent photoluminescence and light transmission of stretched CNC-QNR-PU elastomeric films using a linear polarizer and a crossed polarizer, respectively. To obtain the data,

the light intensity for three samples was collected with the rotation of the sample between polarizers, respectively.

SEM was performed on a Hitachi SU-8230 instrument, using 3 kV accelerating voltage and gold coating. The cross-sections of the films were obtained by cutting the film with a razor blade and attaching the film to the SEM mount.

Supporting Information

Supporting Information is available from the Wiley Online Library or from the author

Acknowledgements

This work is supported by Air Force Research Laboratory FA8650-16-D-5404, the Air Force office of Scientific Research FA9550-20-1-0305, and NSF-CBET 1803495 Awards, and facilities at Georgia Tech Institute for Electronics and Nanotechnology supported by the NSF-ECCS-2025462 Award.

Conflict of Interest

The authors declare no conflict of interest.

Data Availability Statement

Research data are not shared.

Keywords

cellulose nanocrystals, chiral nematic biocomposites, commensurate co-assembly, dynamic chiro-optics, quantum nanorods

Received: May 14, 2021 Revised: June 22, 2021 Published online:

- [1] A. P. Alivisatos, Science 1996, 271, 933.
- [2] C. R. Kagan, E. Lifshitz, E. H. Sargent, D. V. Talapin, *Science* 2016, 353, aac5523.
- [3] J. Yeom, B. Yeom, H. Chan, K. W. Smith, S. Dominguez-Medina, J. H. Bahng, G. Zhao, W.-S. Chang, S.-J. Chang, A. Chuvilin, Nat. Mater. 2015, 14, 66.
- [4] M. V. Mukhina, I. V. Korsakov, V. G. Maslov, F. Purcell-Milton, J. Govan, A. V. Baranov, A. V. Fedorov, Y. K. Gun'ko, Sci. Rep. 2016, 6, 24177.
- [5] J. E. Govan, E. Jan, A. Querejeta, N. A. Kotov, Y. K. Gun'ko, Chem. Commun. 2010, 46, 6072.
- [6] W. Jiang, Z.-b. Qu, P. Kumar, D. Vecchio, Y. Wang, Y. Ma, J. H. Bahng, K. Bernardino, W. R. Gomes, F. M. Colombari, *Science* 2020, 368, 642.
- [7] A. Ben-Moshe, S. G. Wolf, M. B. Sadan, L. Houben, Z. Fan, A. O. Govorov, G. Markovich, Nat. Commun. 2014, 5, 4302.
- [8] S. Li, J. Liu, N. S. Ramesar, H. Heinz, L. Xu, C. Xu, N. A. Kotov, *Nat. Commun.* 2019, 10, 4826.
- [9] W. Ma, L. Xu, A. F. de Moura, X. Wu, H. Kuang, C. Xu, N. A. Kotov, Chem. Rev. 2017, 117, 8041.



www.advancedsciencenews.com www.afm-journal.de

[39] R. Xiong, S. Yu, S. Kang, K. M. Adstedt, D. Nepal, T. J. Bunning,

Z. Tang, J. Am. Chem. Soc. 2017, 139, 8734.
[11] U. Tohgha, K. K. Deol, A. G. Porter, S. G. Bartko, J. K. Choi, B. M. Leonard, K. Varga, J. Kubelka, G. Muller, M. Balaz, ACS Nano 2013, 7, 11094.

[10] X. Gao, X. Zhang, K. Deng, B. Han, L. Zhao, M. Wu, L. Shi, J. Lv,

- 2013, 7, 11094.[12] J. Cheng, J. Hao, H. Liu, J. Li, J. Li, X. Zhu, X. Lin, K. Wang, T. He, ACS Nano 2018. 12. 5341.
- [13] Y. Xia, Y. Zhou, Z. Tang, Nanoscale 2011, 3, 1374.
- [14] R. J. Hafner, L. Tian, J. C. Brauer, T. Schmaltz, A. Sienkiewicz, S. Balog, V. Flauraud, J. Brugger, H. Frauenrath, ACS Nano 2018, 12, 9116.
- [15] M. V. Mukhina, V. G. Maslov, A. V. Baranov, A. V. Fedorov, A. O. Orlova, F. Purcell-Milton, J. Govan, Y. K. Gun'ko, Nano Lett. 2015, 15, 2844.
- [16] L. Wang, A. M. Urbas, Q. Li, Adv. Mater. 2020, 32, 1801335.
- [17] K. E. Shopsowitz, H. Qi, W. Y. Hamad, M. J. MacLachlan, *Nature* 2010, 468, 422.
- [18] J. P. Lagerwall, C. Schütz, M. Salajkova, J. Noh, J. H. Park, G. Scalia, L. Bergström, NPG Asia Mater 2014, 6, e80.
- [19] X. Yang, X. Jin, T. Zhao, P. Duan, Mater. Chem. Front. 2021, 5, 4821.
- [20] J. A. Kelly, M. Giese, K. E. Shopsowitz, W. Y. Hamad, M. J. MacLachlan, Acc. Chem. Res. 2014, 47, 1088.
- [21] R. Xiong, S. Yu, M. J. Smith, J. Zhou, M. Krecker, L. Zhang, D. Nepal, T. J. Bunning, V. V. Tsukruk, ACS Nano 2019, 13, 9074.
- [22] H. Yu, B. Zhao, J. Guo, K. Pan, J. Deng, J. Mater. Chem. C 2020, 8, 1459.
- [23] Y. Shi, Z. Zhou, X. Miao, Y. J. Liu, Q. Fan, K. Wang, D. Luo, X. W. Sun, J. Mater. Chem. C 2020, 8, 1048.
- [24] W. Li, M. Xu, C. Ma, Y. Liu, J. Zhou, Z. Chen, Y. Wang, H. Yu, J. Li, S. Liu, ACS Appl. Mater. Interfaces 2019, 11, 23512.
- [25] R. Xiong, J. Luan, S. Kang, C. Ye, S. Singamaneni, V. V. Tsukruk, Chem. Soc. Rev. 2020, 49, 983.
- [26] H. Zheng, W. Li, W. Li, X. Wang, Z. Tang, S. X. A. Zhang, Y. Xu, Adv. Mater. 2018, 30, 1705948.
- [27] M. Xu, C. Ma, J. Zhou, Y. Liu, X. Wu, S. Luo, W. Li, H. Yu, Y. Wang, Z. Chen, J. Mater. Chem. C 2019, 7, 13794.
- [28] M. A. Osipov, M. V. Gorkunov, ChemPhysChem 2014, 15, 1496.
- [29] T. D. Nguyen, W. Y. Hamad, M. J. MacLachlan, Adv. Funct. Mater. 2014, 24, 777.
- [30] A. Bobrovsky, P. Samokhvalov, V. Shibaev, Adv. Opt. Mater. 2014, 2, 1167
- [31] C. C. Cheung, M. Giese, J. A. Kelly, W. Y. Hamad, M. J. MacLachlan, ACS Macro Lett. 2013, 2, 1016.
- [32] H. Thérien-Aubin, A. Lukach, N. Pitch, E. Kumacheva, Angew. Chem. 2015, 127, 5710.
- [33] M. V. Gorkunov, G. A. Shandryuk, A. M. Shatalova, I. Y. Kutergina, A. S. Merekalov, Y. V. Kudryavtsev, R. V. Talroze, M. A. Osipov, Soft Matter 2013, 9, 3578.
- [34] K. Adstedt, E. A. Popenov, K. J. Pierce, R. Xiong, R. Geryak, V. Cherpak, D. Nepal, T. J. Bunning, V. V. Tsukruk, Adv. Funct. Mater. 2020. 30. 2003597.
- [35] Y. Liang, Y. Xie, D. Chen, C. Guo, S. Hou, T. Wen, F. Yang, K. Deng, X. Wu, I. I. Smalyukh, *Nat. Commun.* 2017, 8, 1410.
- [36] A. Nemati, S. Shadpour, L. Querciagrossa, L. Li, T. Mori, M. Gao, C. Zannoni, T. Hegmann, Nat. Commun. 2018, 9, 3908.
- [37] W. Ma, H. Kuang, L. Xu, L. Ding, C. Xu, L. Wang, N. A. Kotov, *Nat. Commun.* 2013, 4, 2689.
- [38] S. Pan, L. He, J. Peng, F. Qiu, Z. Lin, Angew. Chem. 2016, 128, 8828.

- [40] V. F. Korolovych, V. Cherpak, D. Nepal, A. Ng, N. R. Shaikh, A. Grant, R. Xiong, T. J. Bunning, V. V. Tsukruk, *Polymer* 2018, 145, 334
- [41] L. Carbone, C. Nobile, M. De Giorgi, F. D. Sala, G. Morello, P. Pompa, M. Hytch, E. Snoeck, A. Fiore, I. R. Franchini, *Nano Lett.* 2007, 7, 2942.
- [42] G. van Anders, D. Klotsa, N. K. Ahmed, M. Engel, S. C. Glotzer, Proc. Natl. Acad. Sci. USA 2014, 111, E4812.
- [43] R. M. Parker, G. Guidetti, C. A. Williams, T. Zhao, A. Narkevicius, S. Vignolini, B. Frka-Petesic, Adv. Mater. 2018, 30, 1704477.
- [44] B. Natarajan, J. W. Gilman, Philos. Trans. R. Soc., A 2018, 376, 20170050.
- [45] J. Gong, G. Li, Z. Tang, Nano Today 2012, 7, 564.

V. V. Tsukruk, Adv. Mater. 2020, 32, 1905600.

- [46] L. Onsager, Ann. N. Y. Acad. Sci. 1949, 51, 627.
- [47] M. Adams, Z. Dogic, S. L. Keller, S. Fraden, Nature 1998, 393, 349.
- [48] C. P. Lapointe, T. G. Mason, I. I. Smalyukh, *Science* **2009**, *326*, 1083
- [49] K. L. Young, M. L. Personick, M. Engel, P. F. Damasceno, S. N. Barnaby, R. Bleher, T. Li, S. C. Glotzer, B. Lee, C. A. Mirkin, Angew. Chem., Int. Ed. 2013, 52, 13980.
- [50] S. N. Raja, A. J. Luong, W. Zhang, L. Lin, R. O. Ritchie, A. P. Alivisatos, Chem. Mater. 2016, 8, 2540.
- [51] A. Dufresne, Mater. Today 2013, 16, 220.
- [52] O. Kose, A. Tran, L. Lewis, W. Y. Hamad, M. J. MacLachlan, Nat. Commun. 2019, 10, 510.
- [53] T. Y. Choi, B.-U. Hwang, B.-Y. Kim, T. Q. Trung, Y. H. Nam, D.-N. Kim, K. Eom, N.-E. Lee, ACS Appl. Mater. Interfaces 2017, 9, 18022.
- [54] S. Ling, D. L. Kaplan, M. J. Buehler, Nat. Rev. Mater. 2018, 3, 18016.
- [55] D. Mousanezhad, B. Haghpanah, R. Ghosh, A. M. Hamouda, H. Nayeb-Hashemi, A. Vaziri, Theor. App. Mech. Lett. 2016, 6, 81.
- [56] M. Fortes, M. T. Nogueira, Mater. Sci. Eng.: A 1989, 122, 227.
- [57] G. N. Greaves, A. Greer, R. S. Lakes, T. Rouxel, Nat. Mater. 2011, 10, 823.
- [58] S. N. Fernandes, Y. Geng, S. Vignolini, B. J. Glover, A. C. Trindade, J. P. Canejo, P. L. Almeida, P. Brogueira, M. H. Godinho, *Macromol. Chem. Phys.* 2013, 214, 25.
- [59] E. Nishikawa, H. Finkelmann, H. R. Brand, Macromol. Rapid Commun. 1997, 18, 65.
- [60] W. Ren, P. J. McMullan, A. C. Griffin, Macromol. Chem. Phys. 2008, 209, 1896.
- [61] H. Zheng, B. Ju, X. Wang, W. Wang, M. Li, Z. Tang, S. X. A. Zhang, Y. Xu, Adv. Opt. Mater. 2018, 6, 1801246.
- [62] A. Taniguchi, D. Kaji, N. Hara, R. Murata, S. Akiyama, T. Harada, A. Sudo, H. Nishikawa, Y. Imai, RSC Adv. 2019, 9, 1976.
- [63] K. Takaishi, S. Hinoide, T. Matsumoto, T. Ema, J. Am. Chem. Soc. 2019, 141, 11852.
- [64] G. Albano, G. Pescitelli, L. Di Bari, Chem. Rev. 2020, 120, 10145.
- [65] T. Ohzono, K. Katoh, H. Minamikawa, M. O. Saed, E. M. Terentjev, Nat. Commun. 2021, 12, 787.
- [66] W. K. Bae, K. Char, H. Hur, S. Lee, Chem. Mater. 2008, 20, 531.
- [67] M. E. McConney, S. Singamaneni, V. V. Tsukruk, *Polym. Rev.* 2010, 50, 235.
- [68] Hamamatsu Photonics K.K., Quantaurus-QY Absolute PL quantum yield spectrometer, https://www.hamamatsu.com/us/en/product/ type/C11347-11/index.html (accessed: July 2021).